European Journal of Radiology 118 (2019) 231–238

Contents lists available at ScienceDirect

European Journal of Radiology

journal homepage: www.elsevier.com/locate/ejrad

Research article

Radiomic analysis for preoperative prediction of cervical lymph node metastasis in patients with papillary thyroid carcinoma

Wei Lu[a,b,1], Lianzhen Zhong[b,c,1], Di Dong[b,c,1], Mengjie Fang[b,c], Qi Dai[a], Shaoyi Leng[a], Liwen Zhang[b,c], Wei Sun[a], Jie Tian[b,c,d,**], Jianjun Zheng[a,*], Yinhua Jin[a,*]

[a] Department of Medical Imaging, Hwa Mei Hospital, University of Chinese Academy of Sciences, Ningbo, Zhejiang, China
[b] CAS Key Laboratory of Molecular Imaging, Institute of Automation, Chinese Academy of Sciences, Beijing, China
[c] University of Chinese Academy of Sciences, Beijing, China
[d] Beijing Advanced Innovation Center for Big Data-Based Precision Medicine, School of Medicine, Beihang University, Beijing, 100191, China

ARTICLE INFO

Keywords:
Forecasting
Thyroid neoplasms
Lymphatic metastasis

ABSTRACT

Purpose: Cervical lymph node (LN) metastasis of papillary thyroid carcinoma (PTC) is critical for treatment and prognosis. We explored the feasibility of using radiomics to preoperatively predict cervical LN metastasis in PTC patients.

Method: Total 221 PTC patients (training cohort: n = 154; validation cohort: n = 67; divided randomly at the ratio of 7:3) were enrolled and divided into 2 groups based on LN pathologic diagnosis (N0: n = 118; N1a and N1b: n = 88 and 15, respectively). We extracted 546 radiomic features from non-contrast and venous contrast-enhanced computed tomography (CT) images. We selected 8 groups of candidate feature sets by minimum redundancy maximum relevance (mRMR), and obtained 8 radiomic sub-signatures by support vector machine (SVM) to construct the radiomic signature. Incorporating the radiomic signature, CT-reported cervical LN status and clinical risk factors, a nomogram was constructed using multivariable logistic regression. The nomogram's calibration, discrimination, and clinical utility were assessed.

Results: The radiomic signature was associated significantly with cervical LN status ($p < 0.01$ for both training and validation cohorts). The radiomic signature showed better predictive performance than any radiomic sub-signatures devised by SVM. Addition of radiomic signature to the nomogram improved the predictive value (area under the curve (AUC), 0.807 to 0.867) in the training cohort; this was confirmed in an independent validation cohort (AUC, 0.795 to 0.822). Good agreement was observed using calibration curves in both cohorts. Decision curve analysis demonstrated the radiomic nomogram was worthy of clinical application.

Conclusions: Our radiomic nomogram improved the preoperative prediction of cervical LN metastasis in PTC patients.

1. Introduction

Thyroid carcinoma is one of the most common endocrine malignancies [1]. Papillary thyroid carcinoma (PTC) accounts for 89.4% of all thyroid carcinomas [2]. Cervical lymph node (LN) metastasis is a risk factor for distant metastasis and poor survival in PTC patients [3], and also is an indication for total thyroidectomy. Contrarily, considering the excellent prognosis of PTC, ipsilateral lobectomy is

Abbreviations: AUC, Area under the curve; CT, Computed tomography; LASSO, Least absolute shrinkage and selection operator; LN, Lymph node; MRI, Magnetic resonance imaging; NPV, Negative predictive value; PET, Positron emission tomography; PPV, Positive predictive value; PTC, Papillary thyroid carcinoma; RAI, Radioactive iodine; SPECT, Single-photon emission computed tomography; TG, Thyroglobulin; TGAb, Thyroglobulin antibody; TPOAb, Thyroid peroxidase antibody; US, Ultrasonography

* Corresponding authors at: Department of Medical Imaging, Hwa Mei Hospital, University of Chinese Academy of Sciences, No. 41 Northwest Street, Haishu District, Ningbo, Zhejiang, 315010, China.

** Corresponding author at: CAS Key Laboratory of Molecular Imaging, Institute of Automation, Chinese Academy of Sciences, Beijing, 100190, China.

E-mail addresses: luwei19@ucas.ac.cn (W. Lu), zhonglianzhen2018@ia.ac.cn (L. Zhong), di.dong@ia.ac.cn (D. Dong), fangmengjie2015@ia.ac.cn (M. Fang), yxdaiqi@163.com (Q. Dai), lengshaoyi@163.com (S. Leng), zhangliwen2015@ia.ac.cn (L. Zhang), sunwei@ucas.ac.cn (W. Sun), jie.tian@ia.ac.cn (J. Tian), zhengjianjun@ucas.ac.cn (J. Zheng), jinyh@ucas.ac.cn (Y. Jin).

[1] Contributed equally as the first authors.

https://doi.org/10.1016/j.ejrad.2019.07.018
Received 2 April 2019; Received in revised form 8 June 2019; Accepted 16 July 2019

Table 1
Characteristics of patients in the training and validation cohorts.

Characteristics	Training Cohort (N = 154)			Validation Cohort (N = 67)		
	LN Metastasis (+) (N = 74)	LN Mete stasis (-) (N = 80)	p-value	LN Metastasis (+) (N = 29)	LN Metastasis (-) (N = 38)	p-value
Age, mean ± SD, years	42.42 ± 13.71	48.15 ± 1136		45.97 ± 13.29	47.18 ± 11.43	
< 45, No. (%)	45 (60.81)	29 (36.25)	0.004	13 (44.83)	13(34.21)	0.528
≥ 45, No. (%)	29 (39.19)	51 (63.75)		16 (55.17)	25(65.79)	
Sex, No. (%)						
Male	21 (28.38)	8 (10.00)	0.007	7 (24.14)	4 (10.53)	0.247
Female	53 (71.62)	72(90.00)		22 (75.88)	34 (89.47)	
Primary site (Location), No, (%)						
Right lobe	39 (52.70)	46 (57.50)	0.713	13 (44.83)	22 (57.89)	0.337
Left lobe	33 (44.59)	33 (41.25)		15 (51.72)	16 (42.11)	
isthmus	2 (2.70)	1 (1.25)		1 (3.45)	0 (0.00)	
Primary site (Position, S-l), No. (%)						
Superior	15 (20.27)	18 (22.50)	0.013	5 (17.24)	12 (31.58)	0.025
Medium	38 (51.35)	54 (67.50)		13 (44.83)	22 (57.89)	
inferior	21 (28.38)	8(10.00)		11 (37.93)	4 (10.53)	
Primary site (Position, A-P), No, (%)						
Ventral	31 (54.05)	30 (55.00)	0.614	14 (48.28)	14 (38.84)	0.241
Medium	3 (4.05)	6 (7.50)		0 (0.00)	3 (7.39)	
Dorsal	40 (41.89)	44 (37.50)		15 (51.72)	21 (55.26)	
TG, No. (%)						
Normal	53 (71.62)	51 (63.75)	0.578	14 (48.28)	28 (73.68)	0.496
Abnormal	5 (6.76)	8 (10.00)		3 (10.34)	2 (5.26)	
TGAb, No. (%)						
Normal	58 (75.68)	50 (62.50)	0.087	22 (75.86)	22 (57.89)	0.175
Abnormal	5 (6.76)	13 (16.25)		1 (3.45)	6 (15.79)	
TPOAb, No. (%)						
Normal	53 (71.62)	57 (71.25)	0.728	22 (75.86)	24 (63.16)	0.475
Abnormal	8 (10.81)	6 (7.50)		1 (3.45)	4 (10.53)	
T stage. No. (%)						
T1-2	58 (78.38)	67 (83.75)	0.518	23 (79.31)	33 (86.84)	0.623
T3-4	16 (21.62)	13 (16.25)		6 (20.69)	5 (13.16)	
Capsule, No. (%)						
Not involved	58 (78.38)	67 (83.75)	0.518	23 (79.31)	33 (86.84)	0.623
Involved	16 (21.62)	13 (16.25)		6 (20.69)	5 (13.16)	
Calcification, No. (%)						
Negative	58 (75.68)	55 (68.75)	0.437	18 (62.07)	29 (76.32)	0.321
Positive	18 (24.32)	25 (31.25)		11 (37.93)	9 (23.68)	
CT-reported LN status, No. (%)						
LN-negative	14 (18.92)	43 (53.75)	< 0.001	4 (13.79)	18 (47.37)	< 0.001
LN-suspicious	23 (31.08)	22 (27.50)		6 (20.69)	16 (42.10)	
LN-positive	37 (50.00)	15 (18.75)		19 (65.32)	4 (10.53)	

NOTE: Data are n (%) unless otherwise indicated. No significant differences were found between group A (patients without cervical LN metastasis) and group B (patients with cervical LN metastasis) in terms of primary site (location and position A–P), TG, TGAb, TPOAb, T-stage, capsule, or calcification in both the training and validation cohorts ($p > 0.05$). Age and sex were significantly different between groups A and B in the training cohort ($p = 0.004$ and $p = 0.007$, respectively), but not in the validation cohort. Primary site (position S–I) and CT-reported LN status were significantly different between groups A and B in the training cohort ($p = 0.013$ and $p < 0.001$, respectively) as well as in the validation cohort ($p = 0.025$ and $p < 0.001$, respectively). Primary site (position S–I) refers to the upper (superior pole) and lower (inferior pole) positions of the primary tumor in the thyroid. Primary site (position A–P) refers to the front (anterior or ventral) and back (posterior or dorsal) positions of the primary tumor in the thyroid.

recommended for unifocal tumor smaller than 4 cm and without extrathyroidal extension or LN metastasis to reduce the operative complications [4–6]. A previous study showed that the distant metastasis rates and cancer-specific mortalities had no significant difference between these patients in early stage treated by unilateral lobectomy and total thyroidectomy [7]. Moreover, recurrence rates may be as low as 4% in properly selected patients treated with lobectomy alone [8]. However, due to the lack of discriminate features, it remains a problem how to accurately select the patients without LN metastasis for lobectomy. Thus, the accurate preoperative prediction of cervical LN metastasis will provide a basis for individualized treatment decision.

Ultrasonography (US) is the main noninvasive modality to assess cervical LN metastasis for PTC. It has high specificity (85–97.4%) but low sensitivity (36.7–61%) [9–12]. The accuracy is significantly affected by the quality of US system and the experience of operator [13]. Moreover, US is limited when it evaluates inferior cervical LNs [12]. Computed tomography (CT) has similar sensitivity and specificity compared with US [9]. Liu et al. found quantitative assessment of cervical LN metastasis in PTC with dual-energy spectral CT has a high accuracy (82.9%) [13]. Magnetic resonance imaging (MRI) has no radiation; and with noniodinated contrast agents, it will not delay radioactive iodine (RAI) therapy. But MRI is expensive and time-consuming. Gross et al.'s research on detecting cervical LN metastasis by MRI showed extreme sensitivity (95%) but low specificity (51%) [14], while in a similar study Chen et al. obtained an opposite result with limited sensitivity (33–56%) but high specificity (90–93%) [15]. Single-photon emission computed tomography (SPECT) and positron emission tomography (PET)/CT are extremely sensitive and specific in detecting LN metastasis [16,17]. However, SPECT has a low spatial resolution and PET/CT did not show a significant advantage over US or CT in preoperative prediction of LN metastasis [10,18]. Therefore, accurate preoperative assessment of LN metastasis is still challenging in PTC.

Radiomics is a novel quantitative method, which extracts and analyzes high-dimensional information form medical images for diagnosis and prognosis [19–21]. Radiomics can serve as an imaging biomarker for gene expression [22,23], LN or distant metastasis [24–26],

Table 2
Associations between the actual cervical LN statuses vs. the clinicopathological risk predictors and CT-reported LN statuses.

Characteristics	Training Cohort (N = 154)	Validation Cohort (N = 67)	*P-value*
Age, mean ± SD, years	45.40 ± 12.83	46.66 ± 12.19	
< 45. No. (%)	74 (48.05)	26 (38.81)	0.262
≥ 245. No. (%)	80 (51.95)	41 (61.19)	
Sex. No. (%)			
Male	29 (18.83)	11 (16.42)	0.812
Female	125 (81.17)	56 (83.58)	
Primary site (Location). No. (%)			
Right lobe	85 (55.19)	35 (52.24)	0.881
Left lobe	66 (42.86)	31 (46.27)	
Isthmus	3 (1.95)	1 (1.49)	
Primary site (Position. S-I), No. (%)			
Superior	33 (21.43)	17 (25.37)	0.584
Medium	92 (59.74)	35 (52.24)	
Inferior	29 (18.83)	15 (22.39)	
Primary site (Position. A-P), No. (%)			
Ventral	61 (39.61)	28 (41.79)	0.895
Medium	9 (5.84)	3 (4.48)	
Dorsal	84 (54.55)	36 (53.73)	
TG, No. (%)			
Normal	104 (67.53)	42 (62.69)	1.000
Abnormal	13 (8.44)	5 (7.46)	
TGAb, No. (%)			
Normal	106 (68.83)	44 (65.67)	1.000
Abnormal	18 (11.69)	7 (10.45)	
TPOAb, No. (%)			
Normal	110 (71.43)	46 (68.66)	0.984
Abnormal	14 (9.09)	5 (7.46)	
T stage, No. (%)			
T1-2	125 (81.17)	56 (83.58)	0.812
T3-4	29 (18.83)	11 (16.42)	
Capsule, No. (%)			
Not involved	125 (81.17)	56 (83.53)	0.812
Involved	29 (18.83)	11 (16.42)	
Calcification. No. (%)			
Negative	111 (72.08)	47 (70.15)	0.897
Positive	43 (27.92)	20 (29.85)	
CT-reported LN status, No. (%)			
LN-negative	53 (34.42)	21 (31.34)	0.899
LN-suspicious	45 (29.22)	21 (31.34)	
LN-positive	56 (36.36)	25 (37.31)	
LN metastasis. No. (%)			
Negative	80 (51.95)	38 (56.72)	0.613
Positive	74 (48.05)	29 (43.28)	

NOTE: Data are n (%) unless otherwise indicated. No significant differences were found between the training and validation cohorts in terms of age, sex, primary site, TG, TGAb, TPOAb, T-stage, capsule, calcification, CT-reported LN status, or LN metastasis ($p > 0.05$). Primary site (position S-I) refers to the upper (superior pole) and lower (inferior pole) positions of the primary tumor in the thyroid. Primary site (position A–P) refers to the front (anterior or ventral) and back (posterior or dorsal) positions of the primary tumor in the thyroid.

treatment responses [27] and prognosis [28,29] of cancer. In a recent article, the authors used radiomics characteristics of preoperative US images to predict cervical LN metastasis in patients with PTC [30]. However, to our knowledge, CT radiomics has not been applied to assess LN metastasis in PTC patients.

Therefore, this study aimed to explore the feasibility of preoperative prediction of LN metastasis in patients with PTC using CT radiomic analysis.

2. Materials and methods

2.1. Patients

This retrospective study was approved by the ethics committee; the informed consent requirement was waived. A total of 221 patients (male, n = 40; female, n = 181), who underwent surgical treatment between January 2017 and June 2017, were involved in this study. The mean age of patients is 45.78 ± 12.62 years (range, 19–74 years).The selections of surgical treatment for patients with PTC was described in Appendix A1.

The inclusion criteria were: (i) the primary tumor was pathologically proven PTC; (ii) contrast-enhanced CT was performed before surgery; and (iii) patients underwent neck dissection with ipsilateral lobectomy or total thyroidectomy and got pathological diagnosis of LNs.

The exclusion criteria were: (i) the primary tumor was unclear on CT images due to artifacts; (ii) the primary tumor with the longest diameter ≤ 3 mm; (iii) the primary tumor was difficult to segment due to nodular goiter or chronic lymphocytic thyroiditis; and (iv) other malignancies were present.

We excluded small tumors with the longest diameter ≤ 3 mm to get enough tumor volume for analysis. Recruitment pathway for patients in this study was displayed in Figure S1. The patients were divided into 2 groups based on pathologic result of LN after neck dissection: (A) without cervical LN metastasis found (N0 stage, n = 118); and (B) with cervical LN metastasis (N1a stage, n = 88; and N1b stage, n = 15). The description of the N stages can be seen in Appendix A2.

2.2. CT data acquisition

All patients underwent contrast-enhanced CT before surgery with a 16-slice spiral CT scanner (Sensation 16; SIEMENS) or a 64-slice spiral CT scanner (SOMATOM Definition; SIEMENS). The CT scan parameters were as follows: 120 kV; 150–200 mA s; pitch, 1; rotation time, 1.0 s; detector collimation, 16 × 0.75 mm or 64 × 0.6 mm; field of view, 500 × 500 mm; matrix, 512 × 512; and slice thickness, 5.0 mm. After routine unenhanced CT, contrast-enhanced CTs were performed after a delay of 20 s (arterial phase) and 35 s (venous phase) following an intravenous administration of 85 mL of iodinated nonionic contrast agent (iohexol injection, 350 mg I/mL, Yangtze River, Taizhou, China) at a rate of 2.5–3.0 mL/s with a high-pressure syringe (SCT-210; MEDRAD). The unenhanced and venous contrast-enhanced CT images were reconstructed with 3 mm slice thicknesses and 3 mm intervals. All CT images were retrieved from the picture archiving and communication system (eWorld, China).

2.3. Tumor segmentation

One radiologist (W.L.) with over 10 years of experience performed 3-dimensional tumor segmentation on both the unenhanced and venous contrast-enhanced CT images at the same time for cross-reference, with ITK-SNAP software (open source software; www.itksnap.org). To evaluate the feature reproducibility, we selected 30 cases (its Characteristics was shown in Table S1) randomly for double-blinded comparison of manual segmentations by two radiologists (W.L. and Y.H.J.). The interclass correlation coefficient (ICC) was used to measure the inter-observer agreement of the features which were extracted from the 30 segmentations. We considered an ICC greater than 0.75 as a mark of excellent reliability [31].

2.4. CT-reported LN status

The CT-reported LN status was performed by 2 radiologists (W.L. and Y.H.J.) with over 10 years of experience. Based on the NCCN Guidelines and some previous studies [9,11,13], metastatic LNs were

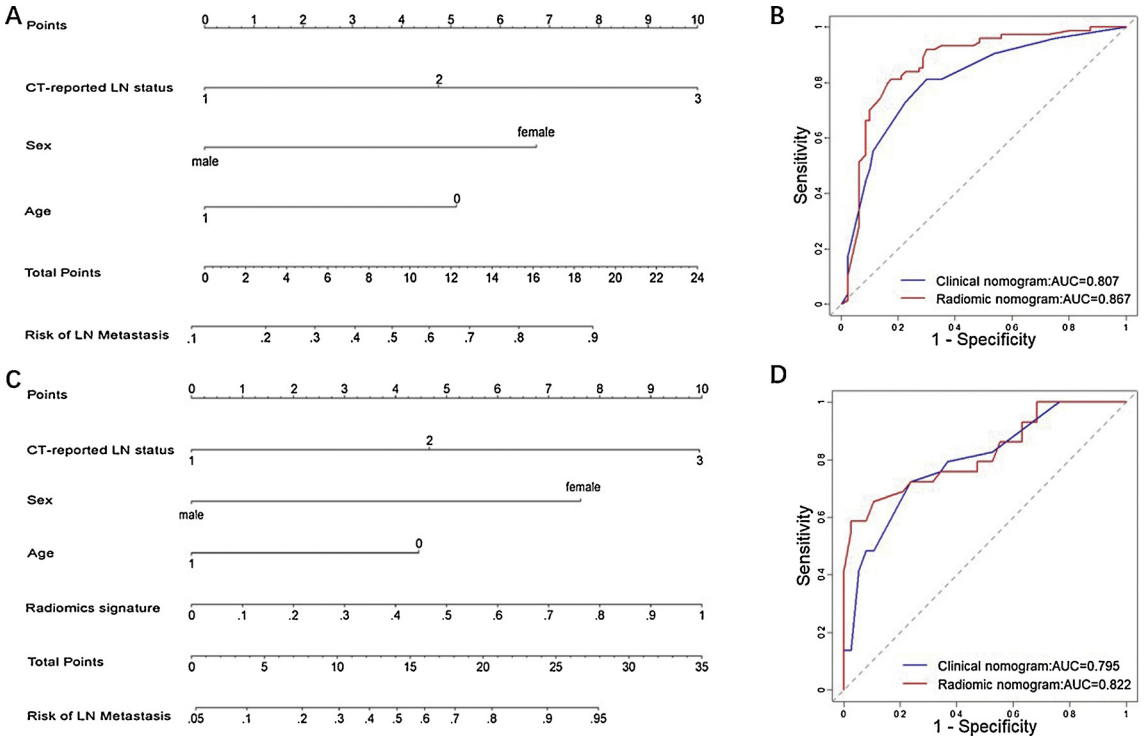

Fig. 1. Comparison between the clinical and radiomic nomograms. (A) The clinical nomogram identified age, sex, and computed tomography (CT)-reported cervical LN status. (B) Receiver operating characteristic (ROC) curves of the clinical nomogram and the radiomic nomogram in the training cohort. (C) The radiomic nomogram was developed by incorporating the radiomic signature into the clinical nomogram. (D) The ROC curves of the radiomic nomogram and the radiomic nomogram in the validation cohort. The nomogram presents binary logistic regression model data to the patient or doctor in an intuitive and clear manner. By comparing (B) and (D), incorporating the radiomic signature into the nomogram shows incremental gains in value for each cohort, especially the training cohort. Thus, the risk of LN metastasis according to the radiomic nomogram is broader than that according to the clinical nomogram.

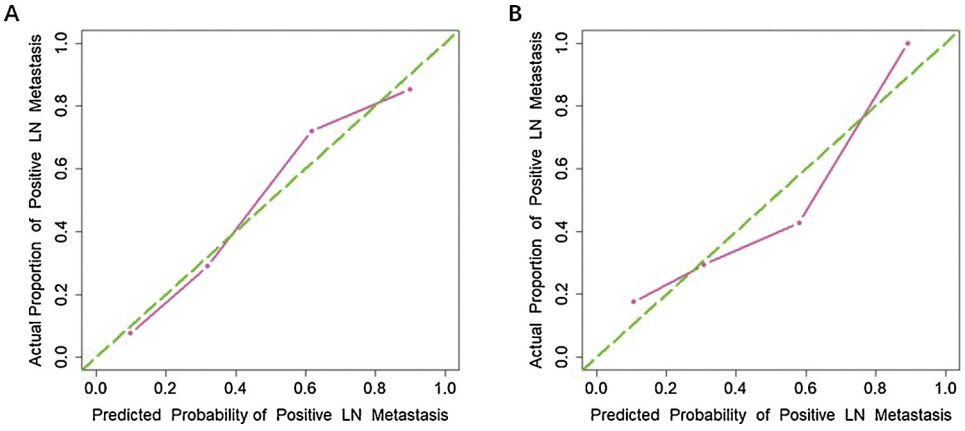

Fig. 2. Calibration curves of the radiomic nomogram in the training and validation cohorts. (A) Calibration curve of radiomic nomogram in the training cohort. The Hosmer-Lemeshow test yielded a nonsignificant statistic (p = 0.378). (B) Calibration curve of radiomic nomogram in the validation cohort. The Hosmer-Lemeshow test also yielded a nonsignificant statistic (p = 0.229). Calibration curves describe the model's calibration in term of agreement between the predicted probability of lymph node (LN) metastasis and observed positive proportion of LN metastasis. The green dashed line represents perfect performance, while the pink solid line presents the actual performance of the radiomic nomogram.

considered when at least one of the following criteria presented: (i) LN ≥ 10 mm in the maximal short axis diameter; (ii) round or irregular shape; (iii) rough margin, fuzzy boundary and/or invasion into adjacent tissues; (iv) calcification or cystic and/or necrotic change; (v) strong enhancement (similar to or stronger than that of the pharyngeal mucosa); and (vi) heterogeneous enhancement. Based on some previous studies [32,33], suspicious LNs were considered when the LNs did not meet the above criteria but were ≥5 mm in the maximal short axial diameter at cervical levels VI.

2.5. Data analysis

We programmed algorithms that were defined in studies by Aerts et al. [22] and Lambin et al. [34] to automatically extract 273 radiomic features from the manually segmented tumor region for each CT scan and a total of 546 features were achieved per patient. These features were derived from first-order statistics features, shape-and-size-based features, statistics-based textural features, and features after wavelet transform (Appendix A3). All feature extraction methods were conducted by MATLAB 2017b (MathWorks, Natick, MA, USA). We chose the minimum redundancy maximum relevance (mRMR) method to select features which were relevant to the actual LN status [35], and then built a classifier based on the selected radiomic features by support vector machine (SVM). We selected 8 groups of feature sets from radiomic features by mRMR, and used SVM to devise them to 8 sub-signatures for prediction (Table S2). We integrated 8 sub-signatures linearly into a radiomic signature. Chalkidou et al. recommended that at least 10 observations per predictor variable in each class were required to have credible estimates for linear models [36]. The sample size of the least class (LN positive patients) in the training cohort is 74

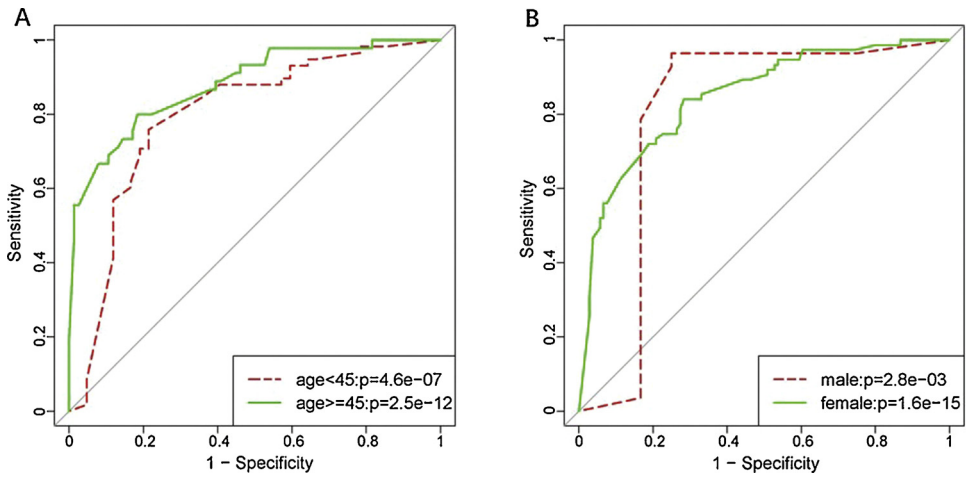

Fig. 3. Stratified analysis of nomogram performance in different subgroups. (A) Stratified analysis in patients with papillary thyroid carcinoma (PTC) according to age. The age cut-off was according to the National Comprehensive Cancer Network (NCCN) Guidelines for thyroid carcinoma (Version 2. 2017). (B) Stratified analysis of nomogram performance in patients with PTC according to sex. These analyses demonstrated that the radiomic nomogram was of practical use in the different subgroups. Detailed results were shown in the supplementary materials.

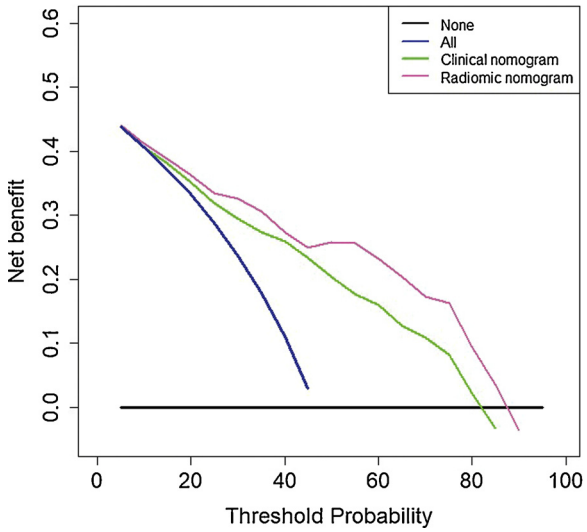

Fig. 4. Decision curve analysis for the clinical and radiomic nomograms. The black solid line represents the assumption that all patients with papillary thyroid carcinoma (PTC) do not have LN metastasis and did not receive treatment. The blue solid line represents the assumption that all patients with PTC have LN metastasis and received treatment. The green solid line represents the assumption that all patients with PTC will receive treatment if the positive probability obtained from clinical nomogram is higher than the threshold probability. The red solid line represents the assumption that all patients with PTC will receive treatment if the positive probability obtained from radiomic nomogram is higher than the threshold probability. The decision curves showed that whatever the threshold probability, using the radiomic nomogram derived in the present study to predict LN metastasis provided a greater benefit than the treat-all-patients approach, treat-none approach, or the clinical nomogram.

and the feature size should be no more than 8. Therefore, we chose 8 sub-signatures for radiomic signature construction.

The potential association of radiomic signature with cervical LN metastasis was evaluated in the training cohort by Mann-Whitney *U* test before being subjected to the validation cohort. Then a multivariable logistic regression (MLR) model included the radiomic signature and the following candidate clinical risk factors: CT-reported LN status, age, sex, and primary site. Backward step-wise selection was applied by using the Wald test until p-value of coefficients of remained parameters was below 0.05. To provide clinicians with a quantitative tool to predict the individual probability of positive cervical LN metastasis, we adopted a nomogram to visualize the outcomes based on the MLR model [37].

The predictive performances of the clinical and radiomic nomograms were evaluated in the training cohort and then tested in the validation cohort. Calibration curves using the radiomic nomogram were obtained in both cohorts and then assessed by Hosmer-Lemeshow test [38]. Stratified analyses were performed to test the nomogram's predictive ability in various subgroups of the entire dataset. To estimate the apparent incremental utility of the radiomic signature, the clinical usefulness of the radiomic nomogram was assessed through decision curve analysis [39].

2.6. Statistical analysis

Statistical analyses were performed by the R software (http://www.R-project.org). The detailed description of the mRMR method was shown in the supplementary materials (Appendix A4), as are the R packages that were used in this study (Appendix A5). All statistical tests were 2-sided, and *p*-values of < 0.05 were considered significant.

3. Results

The clinical characteristics of the training and validation cohorts were summarized in Table 1. No significant difference was found between the two cohorts in any relevant clinical risk factors. Table 2 shows the associations between the actual cervical LN statuses *vs.* the clinical risk predictors and CT-reported LN statuses. The training and validation cohorts were divided randomly from 221 patients at the ratio of 7:3. The positive cervical LN metastasis rates were 48.1% and 43.3% in the training and validation cohorts, respectively. The accuracy of the subjective CT-reported LN status was 64.7% in the entire dataset (65.6% in the training cohort and 62.7% in the validation cohort) (Appendix A6).

After the intra-observer/inter-observer agreement assessment, 447 (81.9%) radiomic features with ICC > 0.75 were reserved for subsequent analysis (Appendix A7, Figure S2). Of these features, 8 groups of feature sets were screened out with our mRMR algorithm. Eight radiomic sub-signatures then were generated by a SVM classifier with a radial basis function. The radiomic signature was a linear combination of eight sub-signatures and the weights of the radiomic sub-signatures for the radiomic signature were calculated based on their accuracies; the signature calculation equation is shown in the supplementary materials (Appendix A8). The radiomic signature performed better than the best radiomic sub-signature (AUC, 0.759 vs. 0.744; accuracy, 73.4% vs. 71.4%), and better performance was achieved in the validation cohort (AUC, 0.706 vs. 0.703; accuracy, 64.2% vs. 62.7%).

The association between the radiomic signature and LN metastasis was significant in the training cohort ($p < 0.001$) and confirmed in the validation cohort ($p = 0.008$). The radiomic signature yielded a value comparable to the CT-reported cervical LN status with respect to the

AUC and accuracy, and showed a good balance between sensitivity and specificity in both cohorts (detailed description was shown in Table S3); this demonstrated the signature's outstanding representation of cervical LN metastasis in patients with PTC. Binary logistic regression analysis identified the radiomic signature, CT-reported LN status, sex, and age as independent variables to construct a radiomic nomogram. In the training cohort, this nomogram performed better than that without the radiomic signature (AUC, 0.867 vs. 0.807) (Fig. 1). The calibration curve for the probability of cervical LN metastasis as estimated by the radiomic nomogram showed good agreement with the actually observed metastasis ($p = 0.378$) (Fig. 2A). In the validation cohort, the clinical nomogram yielded an AUC of 0.795, which increased to 0.822 when incorporating the radiomic signature. In the calibration curves, good agreement ($p = 0.229$) was found between the nomogram-predicted LN metastasis and pathologically proven ones (Fig. 2B). Stratified analysis also showed that the radiomic nomogram had good performance in the different subgroups (Fig. 3 and Table S4). In decision curve analyses, the radiomic nomogram presented the greatest net benefit regardless of the threshold probability in predicting LN metastasis (Fig. 4).

4. Discussion

Cervical LN metastasis is an important criterion for choosing the proper clinical operations, but current methods of predicting LN metastasis status have extremely unbalanced specificity and sensitivity such as US [9–12] and MRI [14]. In this study, we developed a CT radiomic nomogram to improve the accuracy in predicting LN metastasis, with a balanced sensitivity (72.4%) and specificity (76.3%). The radiomic nomogram showed good predictive ability of LN metastasis on both training and independent validation cohorts. Good agreement was also observed using calibration curves in all cohorts. In our cohorts, 32 patients received therapeutic neck dissection of involved compartments for abnormal LNs which were considered to be malignant in CT reports. However, only 15 cases were pathologically proven to be metastasis. This finding highlights the importance of our study in guiding the neck dissection. The decision curve analysis also demonstrated the potential application value of our radiomic nomogram.

In this study, we used mRMR to select features, because it could provide radiomic features with less redundancies and more credible coefficients in the classifier. The sub-signatures devised by SVM based on 8 groups of feature sets enhanced all outcome measures. Thus, the radiomic signature showed significant association with LN metastasis in both training and validation cohorts. Moreover, the radiomic signature could rival the judgment of 2 radiologists with over 10 years of experience. Interestingly, we found that the radiomic signature performed equally well as the CT-reported LN status. The radiomic signature was based on the high-dimensional and statistical features which were extracted from primary tumors. While the CT-reported LN status was based on the visible CT presentations of the LNs, such as maximal short axis diameter, shape, margin, boundary, calcification, cystic change, necrosis, and enhancement. They provided complementary information from different tissues with different types. It might indicate that the images of primary tumor and LNs had the similar value in diagnosis of LN metastasis.

Although the radiomic signature did not achieve better discrimination than the classifier integrating all clinical prediction categories, incorporating the radiomic signature into the clinical nomogram produced an incremental improvement both in training and validation cohorts. The radiomic nomogram had best net benefit regardless of the threshold probability. The Figure S3 in the Supplementary material shows the ROC curves of the CT-reported LN status, radiomic signature, clinical nomogram, and radiomic nomogram in the training and validation cohorts. We found that the AUC of the radiomic nomogram was better than that of radiomic signature only and clinical nomogram without radiomic signature in both cohorts. It also indicated that combination of the radiomic signature and the CT-reported LN status could increase the accuracy in diagnosis of LN metastasis. The reason may be that the decided features for the radiomic signature were significant association with the actual LN metastasis status of the patient with PTC. For example, entropy is a logarithmic function of the tumor volume, spherical disproportion and uniformity respectively indicates the tumor shape and density/enhancement which associated with tumor heterogeneity. The useful decision curve obtained after incorporating the radiomic signature and clinical risk predictors confirmed this method's value in clinical applications.

We reviewed the cases with high rate of misdiagnosis by radiomic signature, and found many of them with calcification. It may be due to calcification enhancing tumor heterogeneity. We also found LN metastasis in some patients without visible LNs in CT images but with positive predictions by radiomic nomogram. Because the radiomic nomogram reflects a wide range of both radiographic and clinical information, it can give a correct diagnosis even when the metastatic LNs are too small to be seen.

To our knowledge, radiomic studies on PTC are rare, and most of them are based on US texture analysis [40,41]. Kim et al. evaluated the role of US texture analysis in predicting LN metastasis in patients with papillary thyroid microcarcinoma (PTMC) and found none of the parameters was independently associated with LN metastasis [41]. Although CT is less efficient in detecting PTC than US, CT can completely and stereoscopically delineate fixed, bulky, and substernal lesions. Additionally, contrast-enhanced CT can display small LNs more sensitively and clearly than US, and can assess the possibility of metastasis according to the degree of enhancement. The NCCN Guideline also states that iodinated contrast is required for optimal cervical imaging using CT, although using it necessitates delaying RAI. Liu et al. used dual-energy spectral CT to quantitatively assess cervical LN metastasis in PTC [13]. Compared with their study, we had a larger sample size (221 vs. 52), and the AUC in our study (0.822) was similar to theirs (0.811).

There were several limitations in our study. First, this is a retrospective study, the clinical procedures were not identical for all patients, such as the arterial phase images were not used, that might cause potential bias; and further validation of our nomogram should be performed in prospective dataset. Second, the prognosis value of our nomogram as well as radiomic signature should be further investigated in the future (Appendix A9). Third, the data was from a single center, and external validation should be studied. Fourth, this study was based on CT images, the iodinated contrast agents used in contrast-enhanced CT would delay RAI therapy [42]. We are planning to use US and MR images for our further research.

In conclusion, we proposed a novel radiomic nomogram based on preoperative CT. The radiomic nomogram is helpful for improving the preoperative prediction of cervical LN metastasis in PTC patients.

Declaration of Competing Interest

We declare that we have no financial and personal relationships with other people or organizations that can inappropriately influence our work, there is no professional or other personal interest of any nature or kind in any product, service and/or company that could be construed as influencing the position presented in, or the review of, the manuscript entitled, “Radiomic Analysis for Preoperative Prediction of Cervical Lymph Node Metastasis in Patients with Papillary Thyroid Carcinoma”.

Acknowledgments

This work was supported by the National Key R&D Program of China (2017YFC1308700, 2017YFA0205200, 2017YFC1309100), National Natural Science Foundation of China (81771924, 81501616, 81227901, 81671851, 81527805), the Beijing Natural Science

Foundation (L182061), the Bureau of International Cooperation of Chinese Academy of Sciences (173211KYSB20160053), the Instrument Developing Project of the Chinese Academy of Sciences (YZ201502), the Youth Innovation Promotion Association CAS (2017175), the Key R &D Project of Zhejiang Province (2017C03042), the Major Medical and Health Program of Zhejiang Province (WKJ-ZJ-1807), the Public Welfare Technology Application Research Project of Zhejiang Province (2017C35003), Natural Science Foundation of Zhejiang Province (LY18H180011), the Public Welfare Technology Research Project of Zhejiang Province (LGF18H180017), Medical Science and Technology Project of Zhejiang Province (2019320334), and Ningbo Municipal Leading and Top-notch Personnel Training Project (NBLJ201801030).

Appendix A. Supplementary data

Supplementary material related to this article can be found, in the online version, at doi:https://doi.org/10.1016/j.ejrad.2019.07.018.

References

[1] W. Chen, R. Zheng, P.D. Baade, S. Zhang, H. Zeng, F. Bray, A. Jemal, X.Q. Yu, J. He, Cancer statistics in China, 2015, CA Cancer J. Clin. 66 (2) (2016) 115–132, https://doi.org/10.3322/caac.21338.

[2] N. Howlader, A.M. Noone, M. Krapcho, D. Miller, K. Bishop, C.L. Kosary, M. Yu, J. Ruhl, Z. Tatalovich, A. Mariotto, D.R. Lewis, H.S. Chen, E.J. Feuer, K.A. Cronin, SEER Cancer Statistics Review, 1975-2014, Based on November 2016 SEER Data Submission, Posted to the SEER Web Site, April 2017, National Cancer Institute, Bethesda, MD, 2017https://seer.cancer.gov/archive/csr/1975_2014/.

[3] L. Chen, Y. Zhu, K. Zheng, H. Zhang, H. Guo, L. Zhang, K. Wu, L. Kong, W. Ruan, J. Hu, X. Zhang, X. Chen, The presence of cancerous nodules in lymph nodes is a novel indicator of distant metastasis and poor survival in patients with papillary thyroid carcinoma, J. Cancer Res. Clin. Oncol. 143 (6) (2017) 1035–1042, https://doi.org/10.1007/s00432-017-2345-2.

[4] M.E. Cabanillas, D.G. Mcfadden, C. Durante, Thyroid cancer, Lancet 388 (10061) (2016) 2783–2795, https://doi.org/10.1016/S0140-6736(16)30172-6.

[5] B. Cady, Hayes Martin Lecture. Our AMES is true: how an old concept still hits the mark: or, risk group assignment points the arrow to rational therapy selection in differentiated thyroid cancer, Am. J. Surg. 174 (5) (1997) 462–468, https://doi.org/10.1016/s0002-9610(97)00162-1.

[6] A.R. Shaha, Implications of prognostic factors and risk groups in the management of differentiated thyroid cancer, Laryngoscope 114 (3) (2004) 393–402, https://doi.org/10.1097/00005537-200403000-00001.

[7] I.D. Hay, C.S. Grant, E.J. Bergstralh, G.B. Thompson, J.A. van Heerden, J.R. Goellner, Unilateral total lobectomy: is it sufficient surgical treatment for patients with AMES low-risk papillary thyroid carcinoma? Surgery 124 (6) (1998) 958–966, https://doi.org/10.1016/s0039-6060(98)70035-2.

[8] R.M. Tuttle, F. Vaisman, M.D. Tronko, Clinical presentation and clinical outcomes in Chernobyl-related paediatric thyroid cancers: What do we know now? What can we expect in the future? Clin. Oncol. R. Coll. Radiol. (R Coll Radiol) 23 (4) (2011) 268–275, https://doi.org/10.1016/j.clon.2011.01.178.

[9] E. Kim, J.S. Park, K.R. Son, J.H. Kim, S.J. Jeon, D.G. Na, Preoperative diagnosis of cervical metastatic lymph nodes in papillary thyroid carcinoma: comparison of ultrasound, computed tomography, and combined ultrasound with computed tomography, Thyroid 18 (4) (2008) 411–418, https://doi.org/10.1089/thy.2007.0269.

[10] H.S. Jeong, C.H. Baek, Y.I. Son, J.Y. Choi, H.J. Kim, Y.H. Ko, J.H. Chung, H.J. Baek, Integrated 18F-FDG PET/CT for the initial evaluation of cervical node level of patients with papillary thyroid carcinoma: comparison with ultrasound and contrast-enhanced CT, Clin Endocrinol (Oxf) 65 (3) (2006) 402–407, https://doi.org/10.1111/j.1365-2265.2006.02612.x.

[11] J.S. Choi, J. Kim, J.Y. Kwak, M.J. Kim, H.S. Chang, E.K. Kim, Preoperative staging of papillary thyroid carcinoma: comparison of ultrasound imaging and CT, AJR Am. J. Roentgenol. 193 (3) (2009) 871–878, https://doi.org/10.2214/AJR.09.2386.

[12] J.L. Roh, J.Y. Park, J.M. Kim, C.J. Song, Use of preoperative ultrasonography as guidance for neck dissection in patients with papillary thyroid carcinoma, J. Surg. Oncol. 99 (1) (2009) 28–31, https://doi.org/10.1002/jso.21164.

[13] X. Liu, D. Ouyang, H. Li, R. Zhang, Y. Lv, A. Yang, C. Xie, Papillary thyroid cancer: dual-energy spectral CT quantitative parameters for preoperative diagnosis of metastasis to the cervical lymph nodes, Radiology 275 (1) (2015) 167–176, https://doi.org/10.1148/radiol.14140481.

[14] N.D. Gross, J.L. Weissman, J.M. Talbot, P.E. Andersen, M.K. Wax, J.I. Cohen, MRI Detection of cervical metastasis from differentiated thyroid carcinoma, Laryngoscope 111 (11) (2001) 1905–1909, https://doi.org/10.1097/00005537-200111000-00006.

[15] Q. Chen, P. Raghavan, S. Mukherjee, M.J. Jameson, J. Patrie, W. Xin, J. Xian, Z. Wang, P.A. Levine, M. Wintermark, Accuracy of MRI for the diagnosis of metastatic cervical lymphadenopathy in patients with thyroid cancer, Radiol. Med. 120 (10) (2015) 959–966, https://doi.org/10.1007/s11547-014-0474-0.

[16] S.H. Paek, K.H. Yi, S.J. Kim, J.Y. Choi, K.E. Lee, Y.J. Park, D.J. Park, K.W. Kang, J.K. Chung, Feasibility of sentinel lymph node dissection using Tc-99m phytate in papillary thyroid carcinoma, Ann. Surg. Treat. Res. 93 (5) (2017) 240–245, https://doi.org/10.4174/astr.2017.93.5.240.

[17] F. Grünwald, T. Kälicke, U. Feine, R. Lietzenmayer, K. Scheidhauer, M. Dietlein, O. Schober, H. Lerch, K. Brandt-Mainz, W. Burchert, G. Hiltermann, U. Cremerius, H.J. Biersack, Fluorine-18 fluorodeoxyglucose positron emission tomography in thyroid cancer: results of a multicentre study, Eur. J. Nucl. Med. 26 (12) (1999) 1547–1552, https://doi.org/10.1007/s002590050493.

[18] W.H. Choi, Y.A. Chung, E.J. Han, H.S. Sohn, S.H. Lee, Clinical value of integrated [18F]fluoro-2-deoxy-D-glucose positron emission tomography/computed tomography in the preoperative assessment of papillary thyroid carcinoma: comparison with sonography, J Ultras Med 30 (9) (2011) 1267–1273, https://doi.org/10.7863/jum.2011.30.9.1267.

[19] P. Lambin, E. Rios-Velazquez, R. Leijenaar, S. Carvalho, R.G. van Stiphout, P. Granton, C.M. Zegers, R. Gillies, R. Boellard, A. Dekker, H.J. Aerts, Radiomics: extracting more information from medical images using advanced feature analysis, Eur. J. Cancer 48 (4) (2012) 441–446, https://doi.org/10.1016/j.ejca.2011.11.036.

[20] V. Kumar, Y. Gu, S. Basu, A. Berglund, S.A. Eschrich, M.B. Schabath, K. Forster, H.J. Aerts, A. Dekker, D. Fenstermacher, D.B. Goldgof, L.O. Hall, P. Lambin, Y. Balagurunathan, R.A. Gatenby, R.J. Gillies, Radiomics: the process and the challenges, Magn. Reson. Imaging 30 (9) (2012) 1234–1248, https://doi.org/10.1016/j.mri.2012.06.010.

[21] W.L. Bi, A. Hosny, M.B. Schabath, M.L. Giger, N.J. Birkbak, A. Mehrtash, T. Allison, O. Arnaout, C. Abbosh, I.F. Dunn, R.H. Mak, R.M. Tamimi, C.M. Tempany, C. Swanton, U. Hoffmann, L.H. Schwartz, R.J. Gillies, R.Y. Huang, H.J.W.L. Aerts, Artificial intelligence in cancer imaging: clinical challenges and applications, CA Cancer J. Clin. 69 (2) (2019) 127–157, https://doi.org/10.3322/caac.21552.

[22] H.J. Aerts, E.R. Velazquez, R.T. Leijenaar, C. Parmar, P. Grossmann, S. Carvalho, S. Cavalho, J. Bussink, R. Monshouwer, B. Haibe-Kains, D. Rietveld, F. Hoebers, M.M. Rietbergen, C.R. Leemans, A. Dekker, J. Quackenbush, R.J. Gillies, P. Lambin, Decoding tumour phenotype by noninvasive imaging using a quantitative radiomics approach, Nat. Commun. 5 (2014) 4006, https://doi.org/10.1038/ncomms5006.

[23] S. Wang, J. Shi, Z. Ye, D. Dong, D. Yu, M. Zhou, Y. Liu, O. Gevaert, K. Wang, Y. Zhu, H. Zhou, Z. Liu, J. Tian, Predicting EGFR mutation status in lung adenocarcinoma on CT image using deep learning, Eur. Respir. J. 53 (3) (2019) 1800986, , https://doi.org/10.1183/13993003.00986-2018.

[24] Y.Q. Huang, C.H. Liang, L. He, J. Tian, C.S. Liang, X. Chen, Z.L. Ma, Z.Y. Liu, Development and validation of a radiomics nomogram for preoperative prediction of lymph node metastasis in colorectal cancer, J. Clin. Oncol. 34 (18) (2016) 2157–2164, https://doi.org/10.1200/JCO.2015.65.9128.

[25] L. Han, Y. Zhu, Z. Liu, T. Yu, C. He, W. Jiang, Y. Kan, D. Dong, J. Tian, Y. Luo, Radiomic nomogram for prediction of axillary lymph node metastasis in breast cancer, Eur. Radiol. (2019), https://doi.org/10.1007/s00330-018-5981-2.

[26] D. Dong, L. Tang, Z.Y. Li, M.J. Fang, J.B. Gao, X.H. Shan, X.J. Ying, Y.S. Sun, J. Fu, X.X. Wang, L.M. Li, Z.H. Li, D.F. Zhang, Y. Zhang, Z.M. Li, F. Shan, Z.D. Bu, J. Tian, J.F. Ji, Development and validation of an individualized nomogram to identify occult peritoneal metastasis in patients with advanced gastric cancer, Ann. Oncol. 30 (3) (2019) 431–438, https://doi.org/10.1093/annonc/mdz001.

[27] J. Song, J. Shi, D. Dong, M. Fang, W. Zhong, K. Wang, N. Wu, Y. Huang, Z. Liu, Y. Cheng, Y. Gan, Y. Zhou, P. Zhou, B. Chen, C. Liang, Z. Liu, W. Li, J. Tian, A new approach to predict progression-free survival in stage IV EGFR-mutant NSCLC patients with EGFR-TKI therapy, Clin. Cancer Res. 24 (15) (2018) 3583–3592, https://doi.org/10.1158/1078-0432.CCR-17-2507.

[28] B. Zhang, J. Tian, D. Dong, D. Gu, Y. Dong, L. Zhang, Z. Lian, J. Liu, X. Luo, S. Pei, X. Mo, W. Huang, F. Ouyang, B. Guo, L. Liang, W. Chen, C. Liang, S. Zhang, Radiomics features of multiparametric MRI as novel prognostic factors in advanced nasopharyngeal carcinoma, Clin. Cancer Res. 23 (15) (2017) 4259–4269, https://doi.org/10.1158/1078-0432.CCR-16-2910.

[29] Y. Meng, Y. Zhang, D. Dong, C. Li, X. Liang, C. Zhang, L. Wan, X. Zhao, K. Xu, C. Zhou, J. Tian, H. Zhang, Novel radiomic signature as a prognostic biomarker for locally advanced rectal cancer, J. Magn. Reson. Imaging 48 (3) (2018) 605–614, https://doi.org/10.1002/jmri.25968.

[30] T. Liu, S. Zhou, J. Yu, Y. Guo, Y. Wang, J. Zhou, C. Chang, Prediction of lymph node metastasis in patients with papillary thyroid carcinoma: a radiomics method based on preoperative ultrasound images, Technol. Cancer Res. Treat. 18 (2019), https://doi.org/10.1177/1533033819831713.

[31] W.T. Barry, D.N. Kernagis, H.K. Dressman, R.J. Griffis, J.D. Hunter, J.A. Olson, J.R. Marks, G.S. Ginsburg, P.K. Marcom, J.R. Nevins, J. Geradts, M.B. Datto, Intratumor heterogeneity and precision of microarray-based predictors of breast cancer biology and clinical outcome, J. Clin. Oncol. 28 (13) (2010) 2198–2206, https://doi.org/10.1200/JCO.2009.26.7245.

[32] G.W. Randolph, Q.Y. Duh, K.S. Heller, V.A. LiVolsi, S.J. Mandel, D.L. Steward, R.P. Tufano, R.M. Tuttle, American Thyroid Association Surgical Affairs Committee's Taskforce on Thyroid Cancer Nodal Surgery, the prognostic significance of nodal metastasis from papillary thyroid carcinoma can be stratified based on the size and number of metastatic lymph nodes, as well as the presence of extranodal extension, Thyroid 22 (11) (2012) 1144–1152, https://doi.org/10.1089/thy.2012.0043.

[33] Y. Zhao, X. Li, L. Li, X. Wang, M. Lin, X. Zhao, D. Luo, J. Li, Preliminary study on the diagnostic value of single-source dual-energy CT in diagnosing cervical lymph node metastasis of thyroid carcinoma, J. Thorac. Dis. 9 (11) (2017) 4758–4766, https://doi.org/10.21037/jtd.2017.09.151.

[34] P. Lambin, R.T.H. Leijenaar, T.M. Deist, J. Peerlings, E.E.C. de Jong, J. van Timmeren, S. Sanduleanu, R.T.H.M. Larue, A.J.G. Even, A. Jochems, Y. van Wijk, H. Woodruff, J. van Soest, T. Lustberg, E. Roelofs, W. van Elmpt, A. Dekker, F.M. Mottaghy, J.E. Wildberger, S. Walsh, Radiomics: the bridge between medical imaging and personalized medicine, Nat. Rev. Clin. Oncol. 14 (12) (2017) 749–762,

https://doi.org/10.1038/nrclinonc.2017.141.
[35] C. Ding, H. Peng, Minimum redundancy feature selection from microarray gene expression data, J. Bioinform. Comput. Biol. 3 (2) (2005) 185–205, https://doi.org/10.1142/s0219720005001004.
[36] A. Chalkidou, M.J. O'Doherty, P.K. Marsden, False discovery rates in PET and CT studies with texture features: a systematic review, PLoS One 10 (5) (2015) e0124165, https://doi.org/10.1371/journal.pone.0124165.
[37] A. Iasonos, D. Schrag, G.V. Raj, K.S. Panageas, How to build and interpret a nomogram for cancer prognosis, J. Clin. Oncol. 26 (8) (2008) 1364–1370, https://doi.org/10.1200/JCO.2007.12.9791.
[38] P. Paul, M.L. Pennell, S. Lemeshow, Standardizing the power of the Hosmer–Lemeshow goodness of fit test in large data sets, Stat. Med. 32 (1) (2013) 67–80, https://doi.org/10.1002/sim.5525.
[39] A.J. Vickers, E.B. Elkin, Decision curve analysis: a novel method for evaluating prediction models, Med. Decis. Making 26 (6) (2006) 565–574, https://doi.org/10.1177/0272989X06295361.
[40] A.A. Ardakani, A. Gharbali, A. Mohammadi, Classification of benign and malignant thyroid nodules using wavelet texture analysis of sonograms, J. Ultrasound Med. 34 (11) (2015) 1983–1989, https://doi.org/10.7863/ultra.14.09057.
[41] S.Y. Kim, E. Lee, S.J. Nam, E.K. Kim, H.J. Moon, J.H. Yoon, K.H. Han, J.Y. Kwak, Ultrasound texture analysis: association with lymph node metastasis of papillary thyroid microcarcinoma, PLoS One 12 (4) (2017) e0176103, https://doi.org/10.1371/journal.pone.0176103.
[42] R.J. Amdur, E.L. Mazzaferri, Intravenous iodinated contrast effects iodine uptake for months, in: R.J. Amdur, E.L. Mazzaferri (Eds.), Essentials of Thyroid Cancer Management. 1st, Springer, New York, 2005, pp. 211–213.